1 Supporting figures

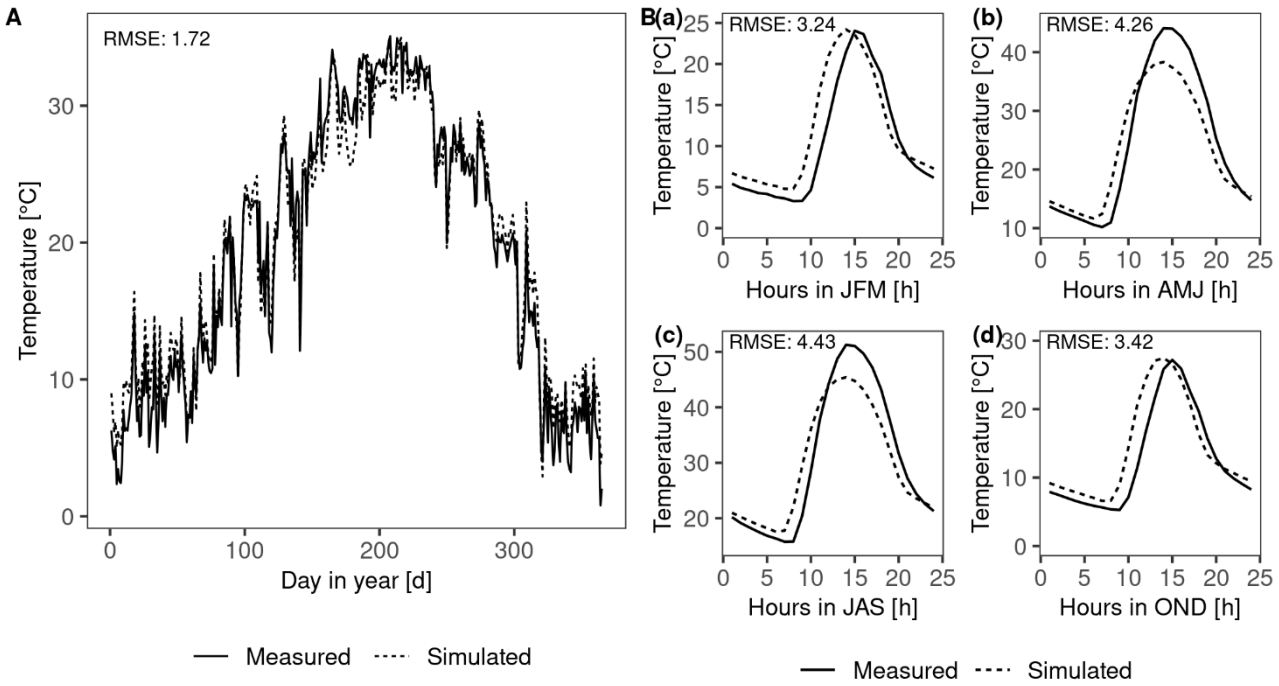

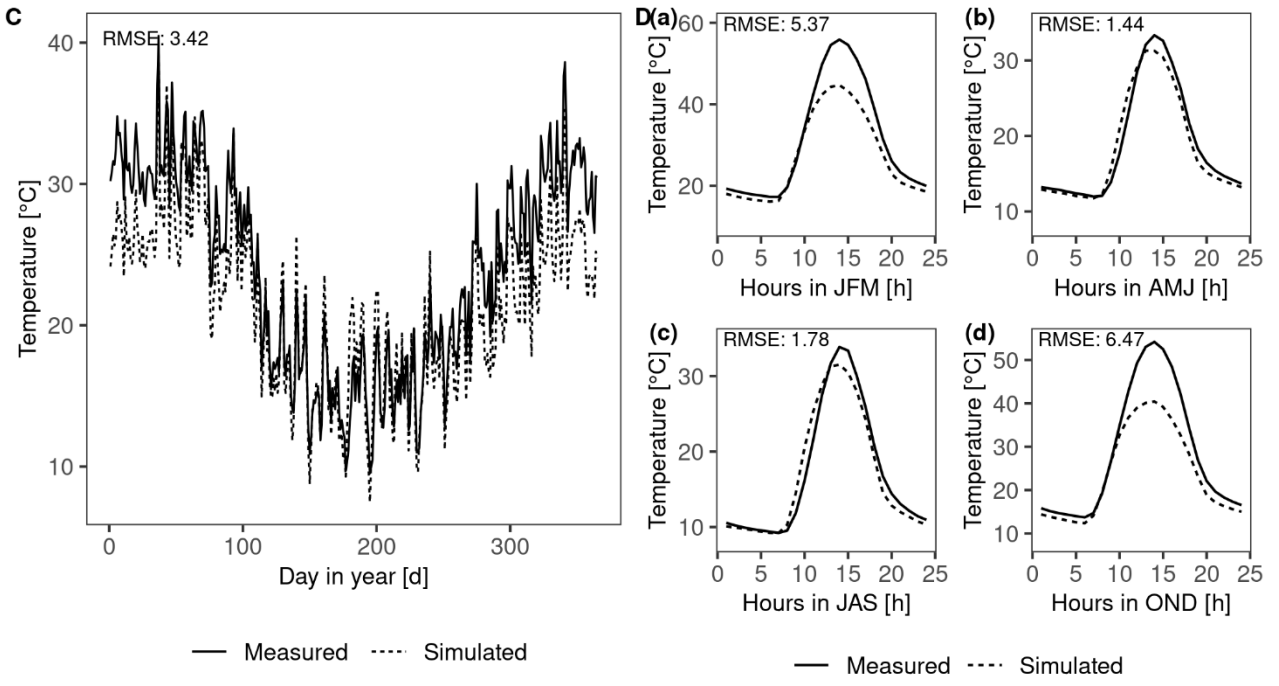

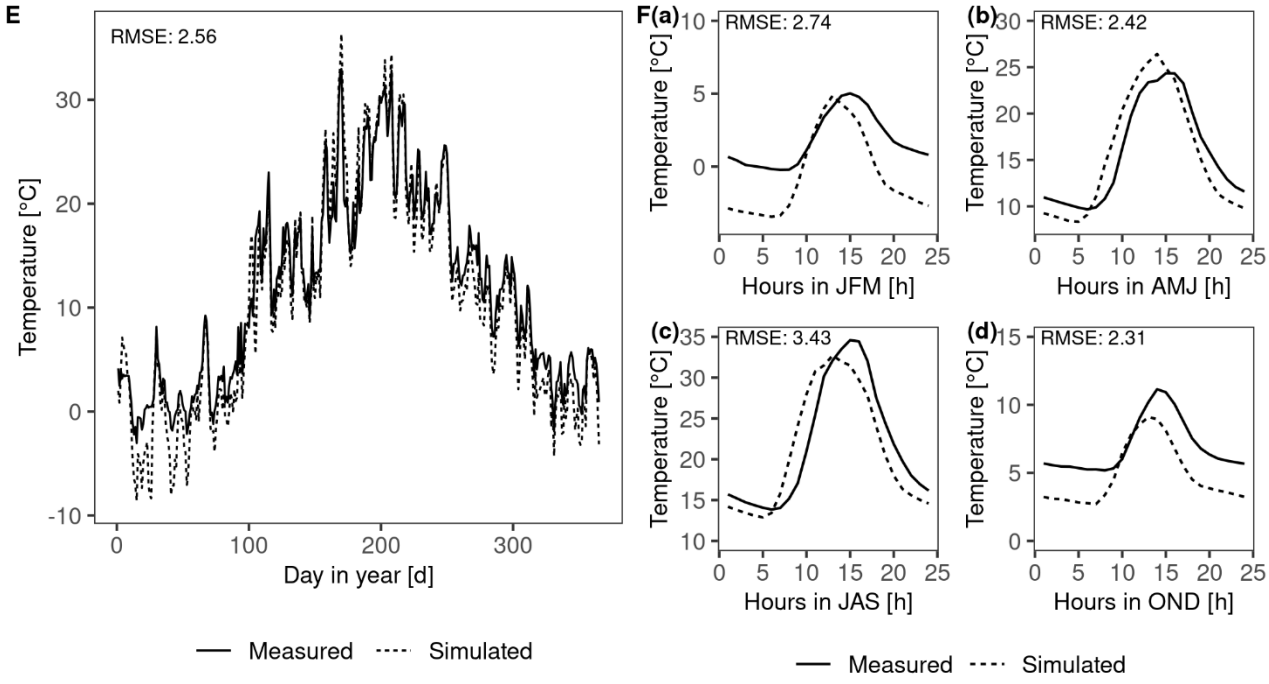
E
RMSE: 2.56
Temperature [°C]
Day in year [d]
Measured
Simulated
F(a)
RMSE: 2.74
Hours in JFM [h]
(b)
RMSE: 2.42
Hours in AMJ [h]
(c)
RMSE: 3.43
Hours in JAS [h]
(d)
RMSE: 2.31
Hours in OND [h]
Measured
Simulated

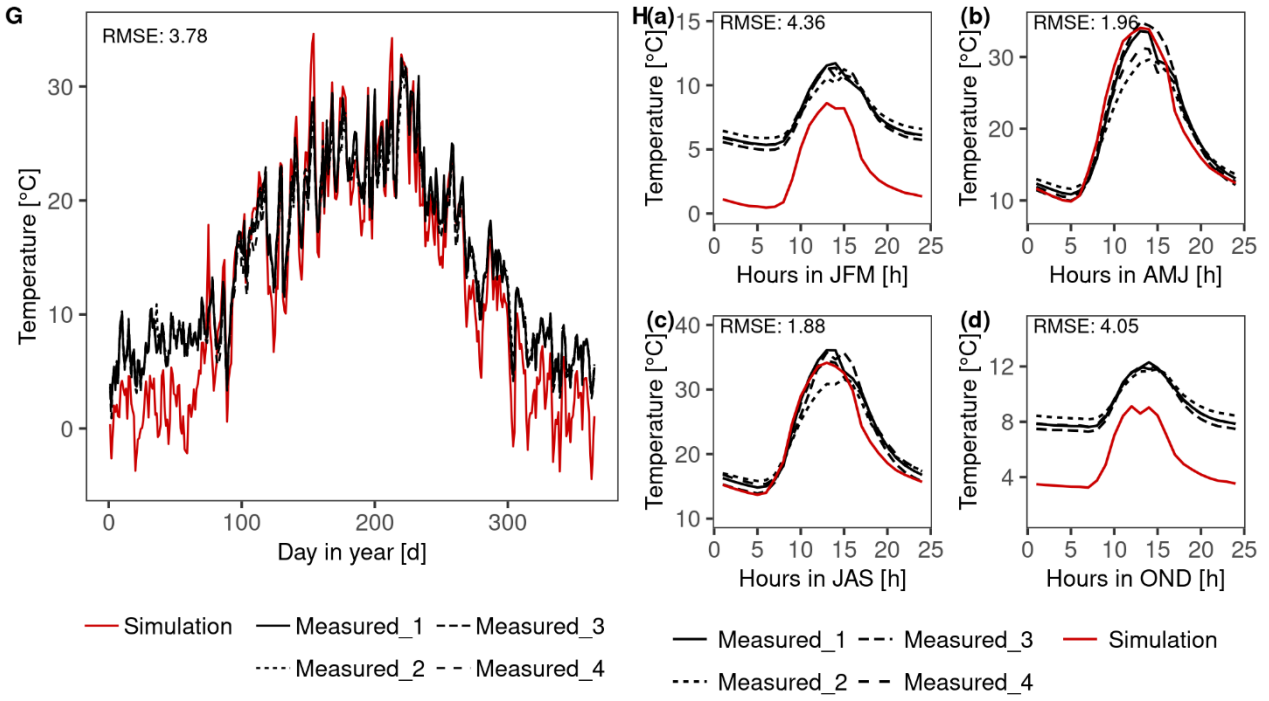
G
RMSE: 3.78
Temperature [°C]
Day in year [d]
Simulation
Measured_1
Measured_3
Measured_2
Measured_4
H(a)
RMSE: 4.36
Hours in JFM [h]
(b)
RMSE: 1.96
Hours in AMJ [h]
(c)
RMSE: 1.88
Hours in JAS [h]
(d)
RMSE: 4.05
Hours in OND [h]
Measured_1
Measured_3
Simulation
Measured_2
Measured_4

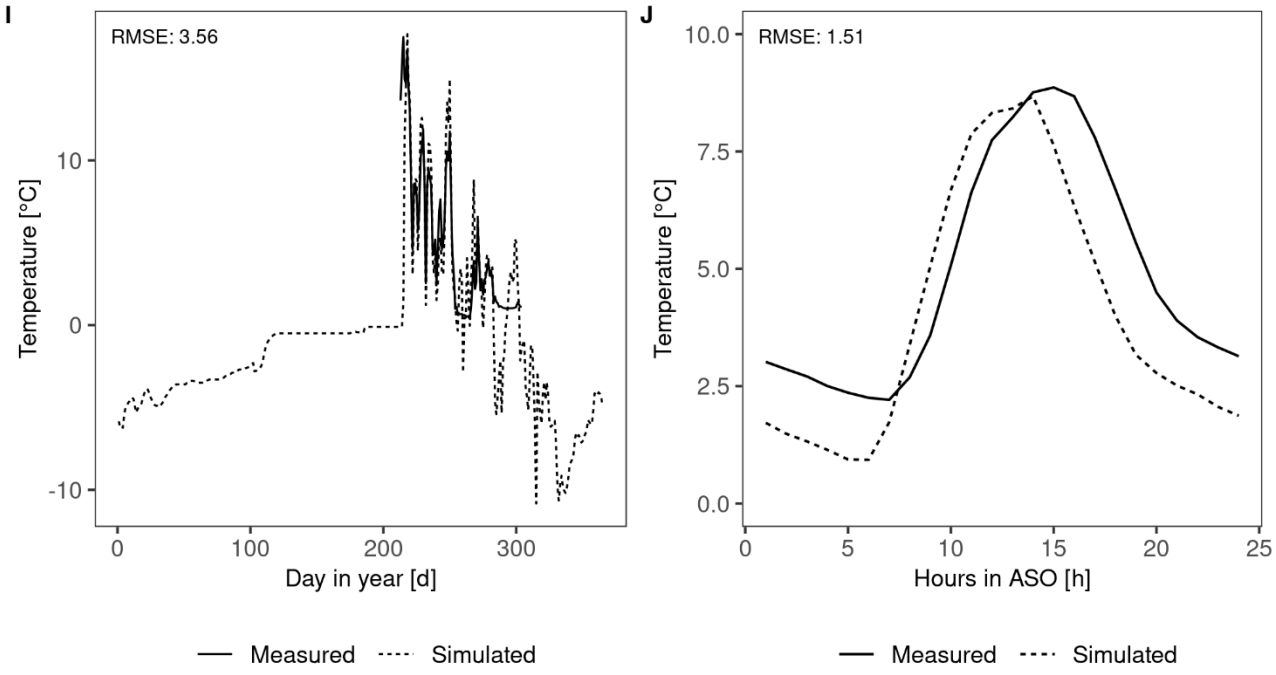

Figure S1: Calibration of abiotic parameters for the data-driven model via comparing the seasonal (left panel) and diurnal (right panel) surface temperature of lichen-dominated biocrusts at sites D1 (A, B), D2 (C, D), T1 (E, F), and A1 (I, J); at site T3 (G, H) the simulated patterns of moss-dominated biocrusts was compared to measured temperature data by four sensors at different locations. In the right panel describing the diurnal patterns (B, D, F, H), the (a), (b), (c) and (d) indicate the comparison of patterns of hourly average data in January, February and March (JFM); April, May and June (AMJ); July, August and September (JAS); October, November and December (OND), respectively. At site A1 (J), the average data was during August, September and October (ASO).

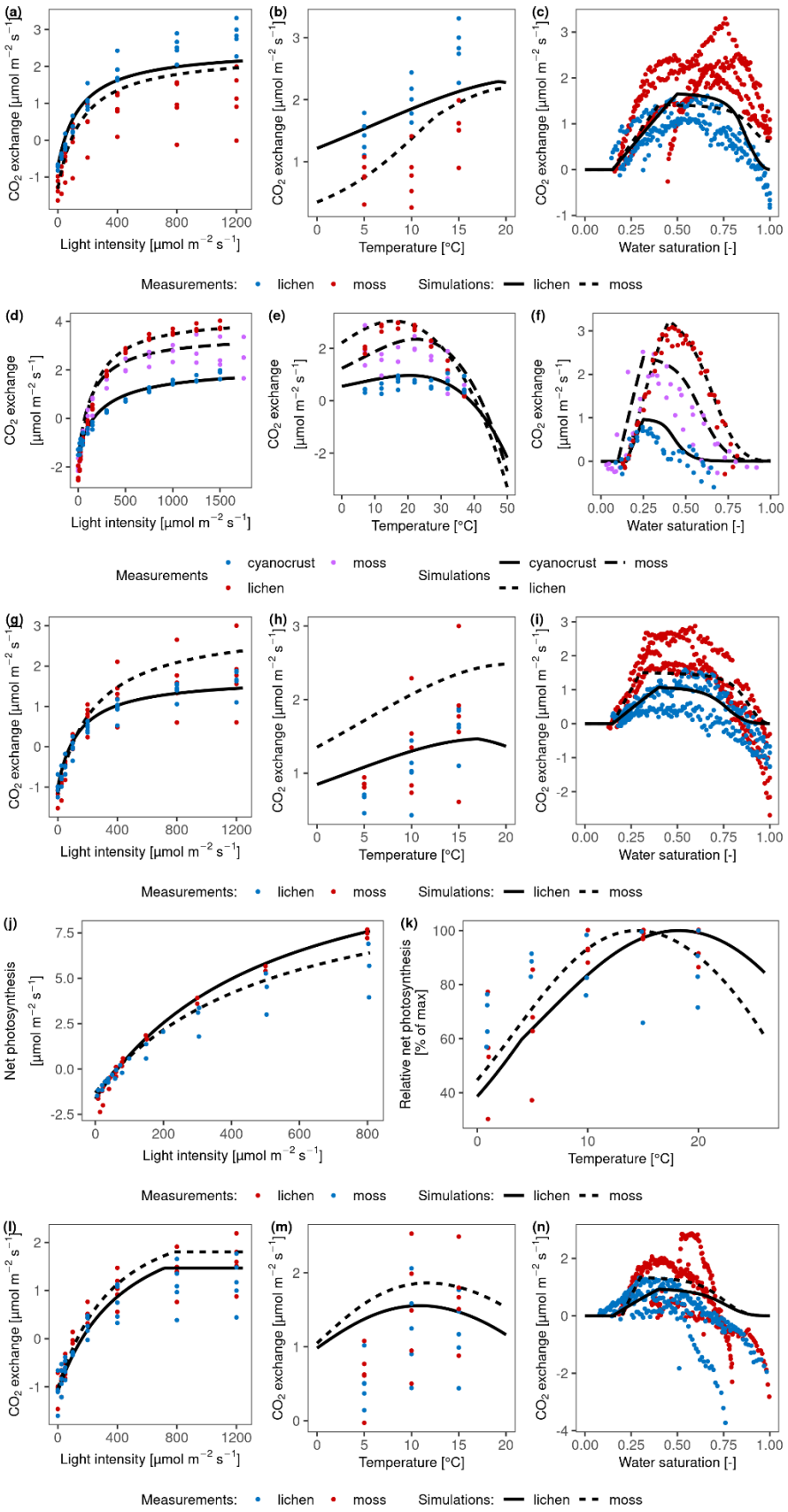

Figure S2: Calibration results of physiological traits for the data-driven model at site D1 (a, b, c), D2 (d, e, f), T1 (g, h, i), T3 (j, k) and A1 (l, m, n), via fitting the photosynthetic response curves to some environmental factors. (a, d, g, j, l): net photosynthesis rate in response to light at optimum water content (OWC) and 15°C at D1, T1 and A1; OWC and 22 °C at D2; water saturation for 30% and 15°C at T3. (b, e, h, k, m): net photosynthesis rate in response to temperature at 1200 µmol m^{-2} s^{-1} light and OWC

at D1, T1 and A1; 500 µmol m^{-2} s^{-1} light and OWC at D2; 1500 µmol m^{-2} s^{-1} light and water saturation for 30% at T3. (c, f, i, n): net photosynthesis rate in response to relative water saturation at 400 µmol m^{-2} s^{-1} light and 15°C at D1, T2 and A1; 500 µmol m^{-2} s^{-1} light and 22 °C at D2.

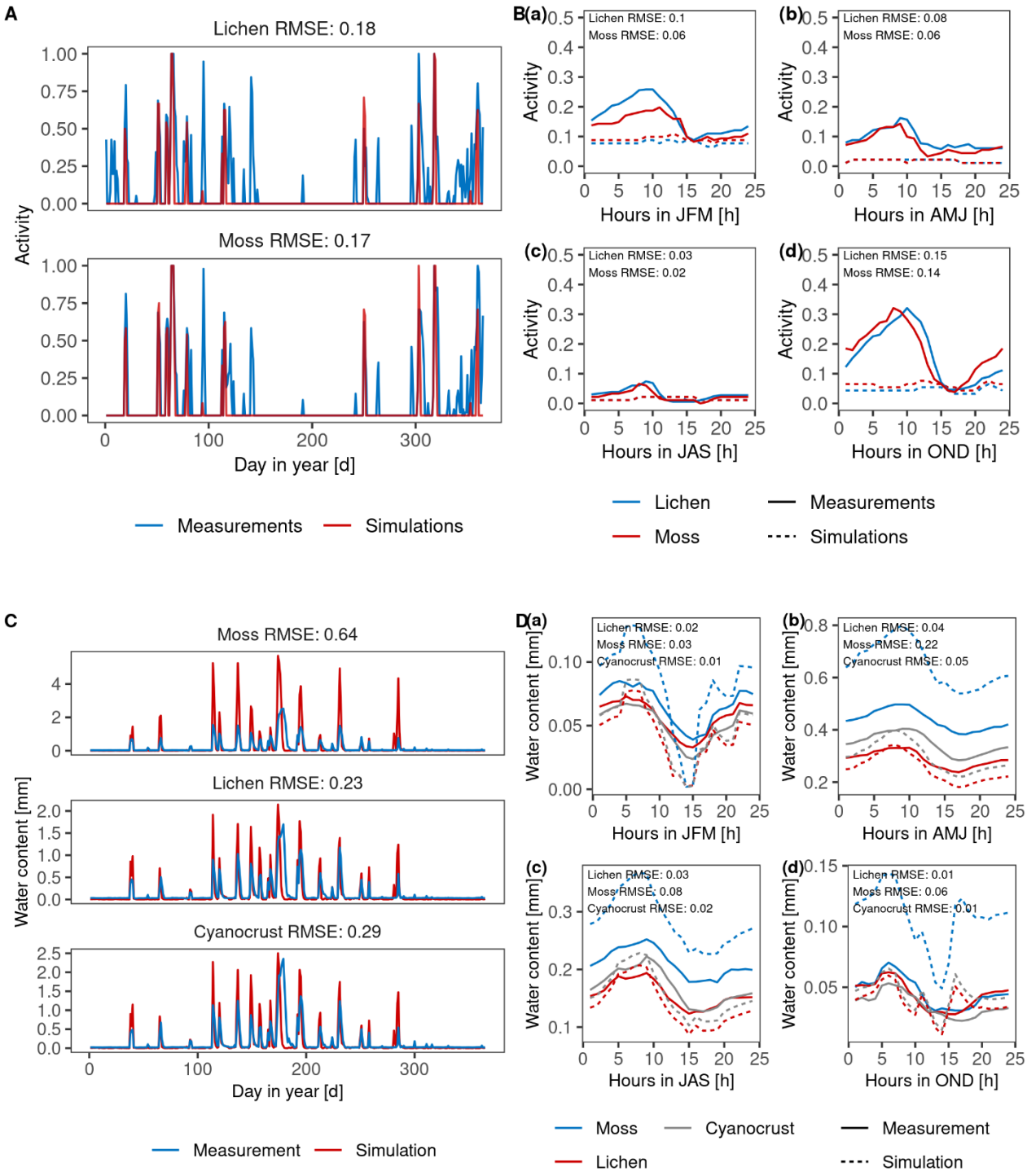

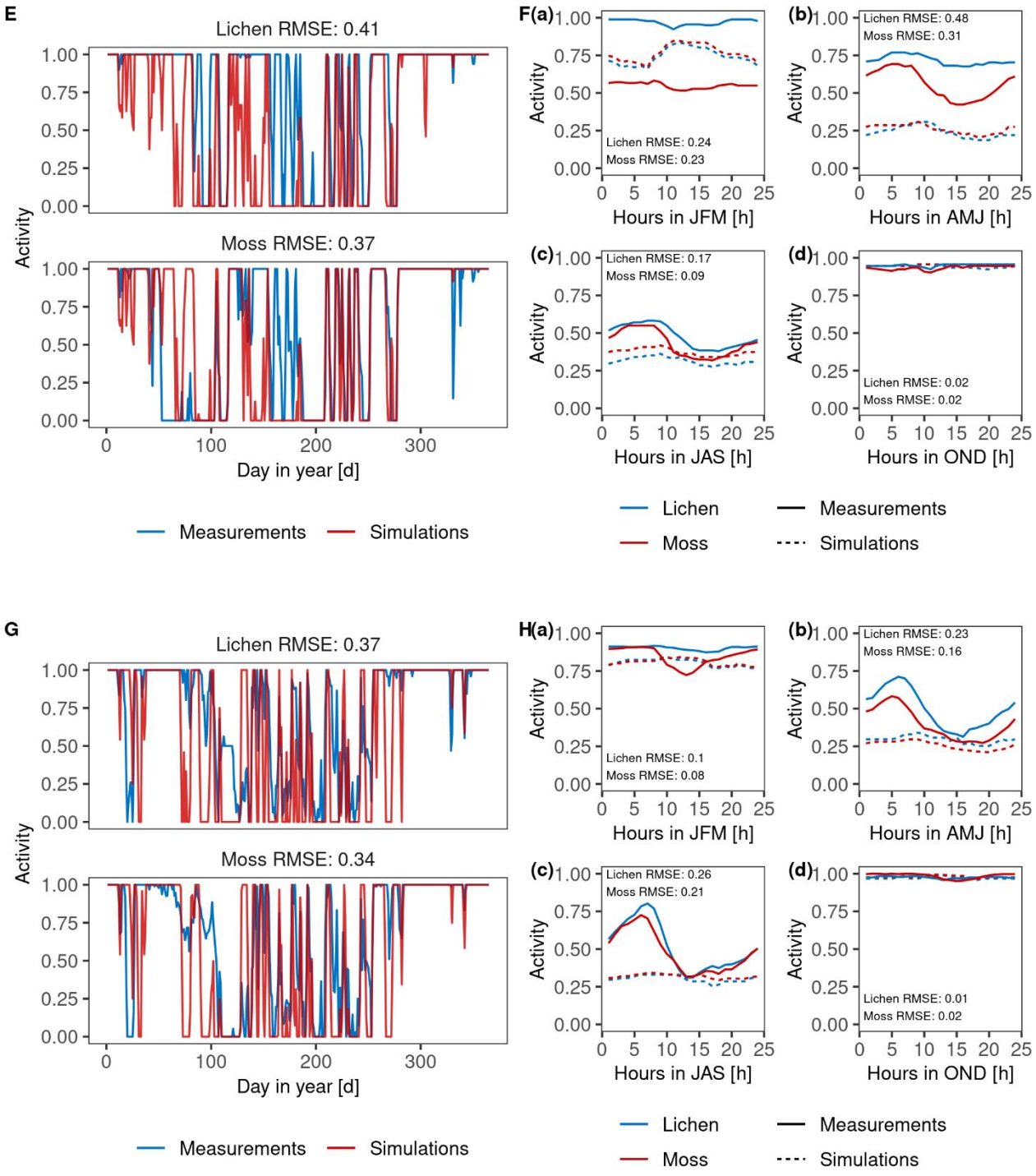
E
Lichen RMSE: 0.41
Moss RMSE: 0.37
Activity
Day in year [d]
Measurements
Simulations
F(a)
Lichen RMSE: 0.24
Moss RMSE: 0.23
(b)
Lichen RMSE: 0.48
Moss RMSE: 0.31
(c)
Lichen RMSE: 0.17
Moss RMSE: 0.09
(d)
Lichen RMSE: 0.02
Moss RMSE: 0.02
Hours in JFM [h]
Hours in AMJ [h]
Hours in JAS [h]
Hours in OND [h]
Lichen
Moss
Measurements
Simulations
G
Lichen RMSE: 0.37
Moss RMSE: 0.34
H(a)
Lichen RMSE: 0.1
Moss RMSE: 0.08
(b)
Lichen RMSE: 0.23
Moss RMSE: 0.16
(c)
Lichen RMSE: 0.26
Moss RMSE: 0.21
(d)
Lichen RMSE: 0.01
Moss RMSE: 0.02

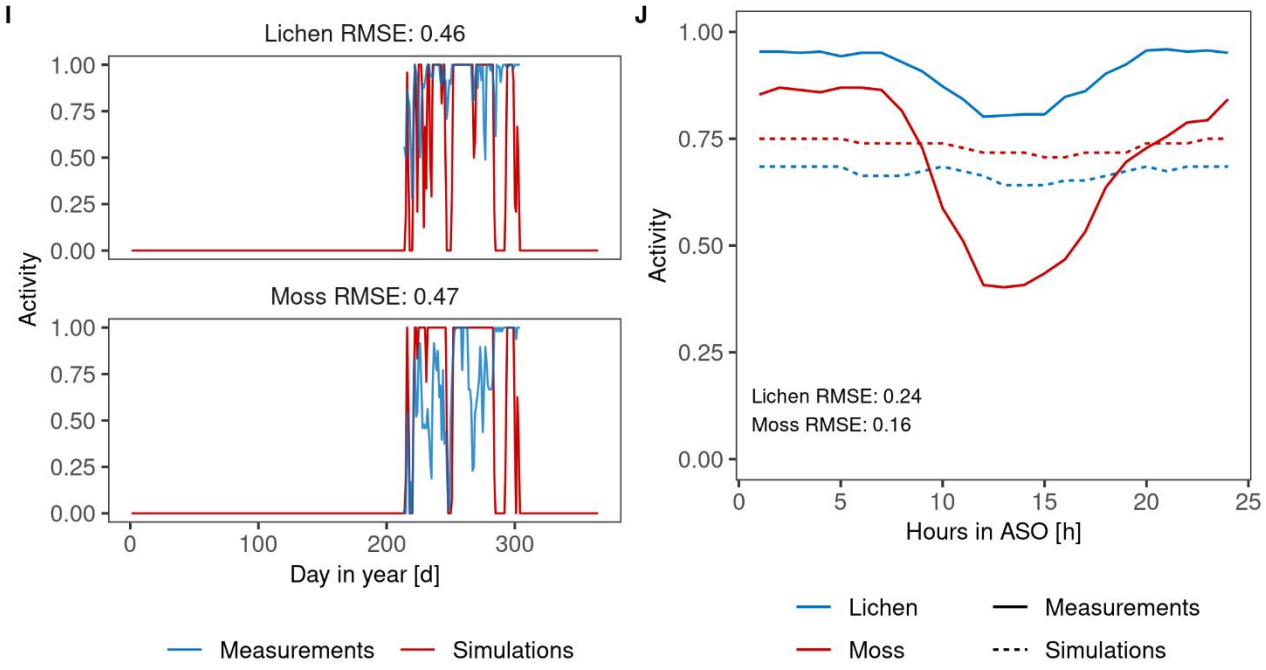

Figure S3: Validation of the water and energy balance in the data-driven model via comparing the seasonal (left panel) and diurnal (right panel) water content at site D2 (C, D) or activity patterns of lichen- and moss-dominated biocrusts at sites D1 (A, B), T1 (E, F), T2 (G, H) and A1 (I, J). In the right panel describing the diurnal patterns (B, D, F, H), the (a), (b), (c) and (d) indicate the comparison of the hourly average data in January, February and March (JFM); April, May and June (AMJ); July, August and September (JAS); October, November and December (OND), respectively. At site A1 (J), the average data was during August, September and October (ASO).

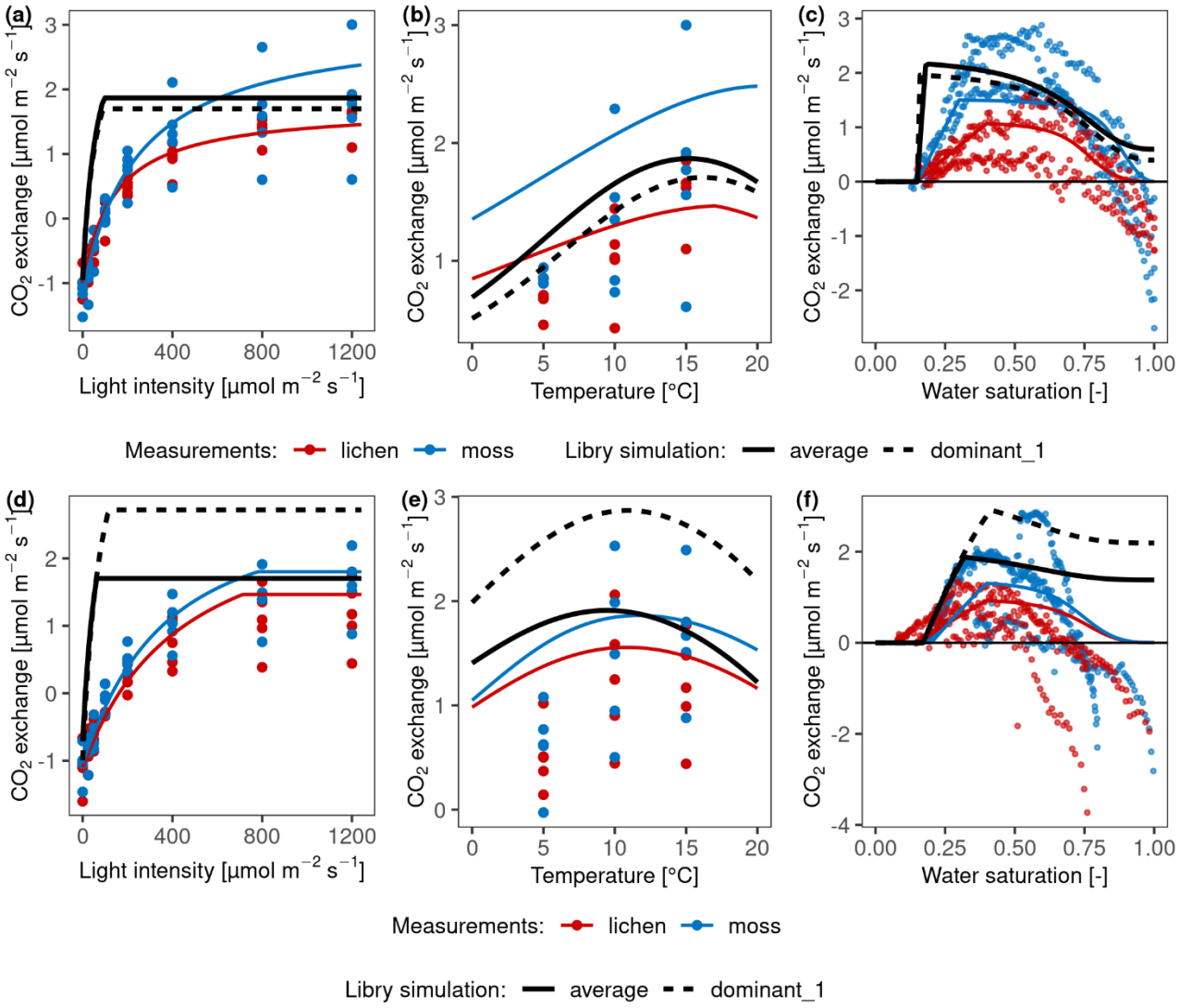

Figure S4: Comparison of photosynthetic performance of dominant strategies selected by LiBry model and the measured data as well as the fitted response curves by data-driven model at site T1 (a, b, c) and A1 (d, e, f). (a, d): photosynthesis relation in response to light intensity; (b, e): photosynthesis relation in response to temperature; (c, f): photosynthesis relation in response to water saturation. The colored points and lines represent the measured and simulated by data-driven model CO_2 exchange rates of moss and lichens. The black lines show the simulated photosynthetic relations of the most dominant strategies with positive C balance selected by LiBry model and the average strategy calculated by LiBry model. The parameter values for the average strategy are the average of the corresponding parameters for all selected surviving strategies.

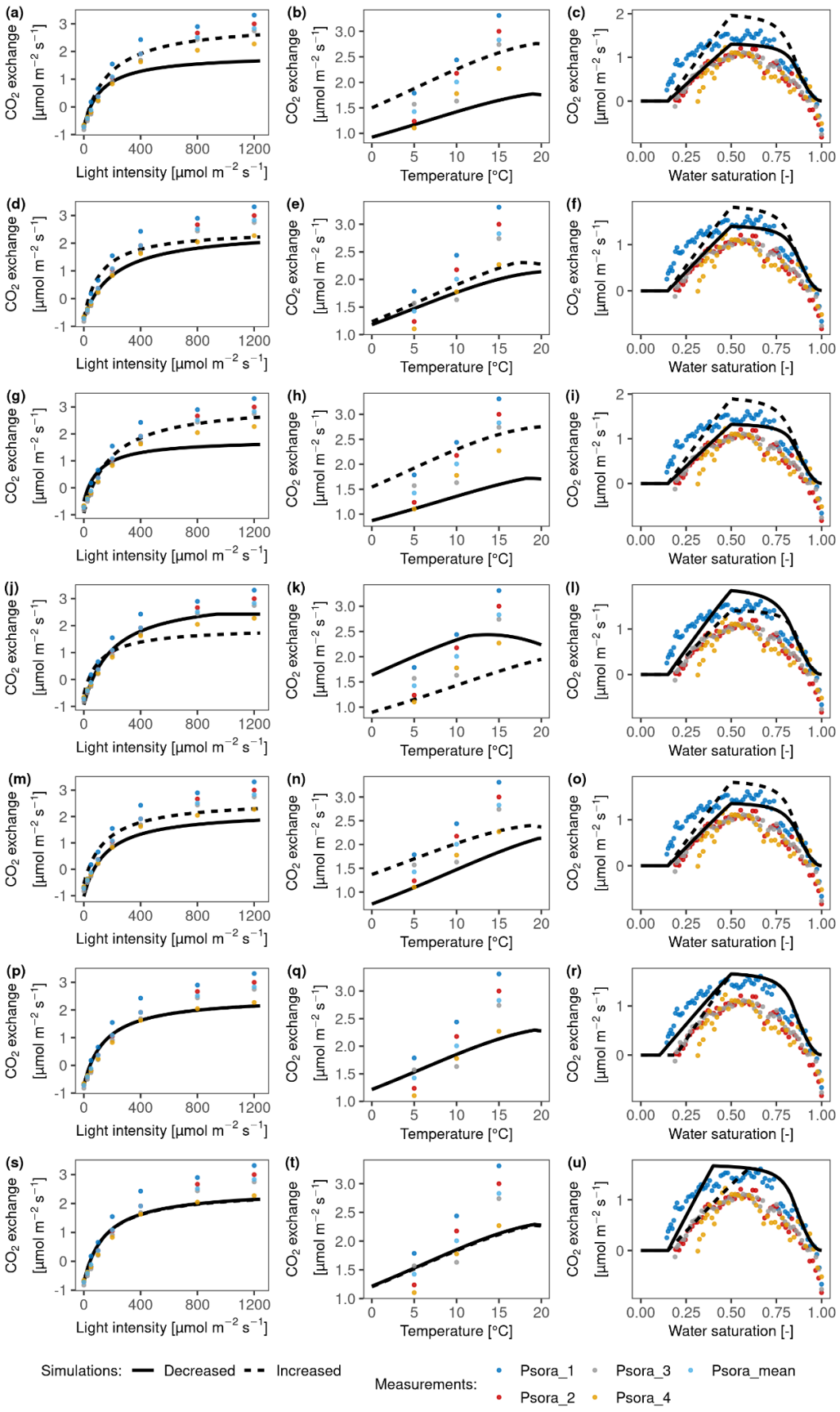

Figure S5: Simulated net photosynthesis rate in response to light (a, d, g, j, m, p, s), temperature (b, e, h, k, n, q, t) and water (c, f, i, l, o, r, u) at site D1 by the data-driven model with decreased or increased physiological parameters. These varying physiological parameters are respiration cost of RuBisCO enzyme (Rub_ratio) (a-c), light absorption fraction in cells (ExtL) (d-f), metabolic respiration cost per surface area (Resp_main) (g-i), the optimum temperature for gross photosynthesis (Topt)

(j-l), Q10 value of respiration (q10) (m-o), minimum saturation for activation (Sat_act0) (p-r) and minimum saturation for full activation (Sat_act1) (s-u). Resp_main, ExtL, q10, Sat_act0 increased or decreased by 30%, Rub_ratio and Sat_act1 by 20%, and Topt by 5 K. The colored points represent the measured CO_2 exchange rates of different replicates of lichen-dominated biocrusts.

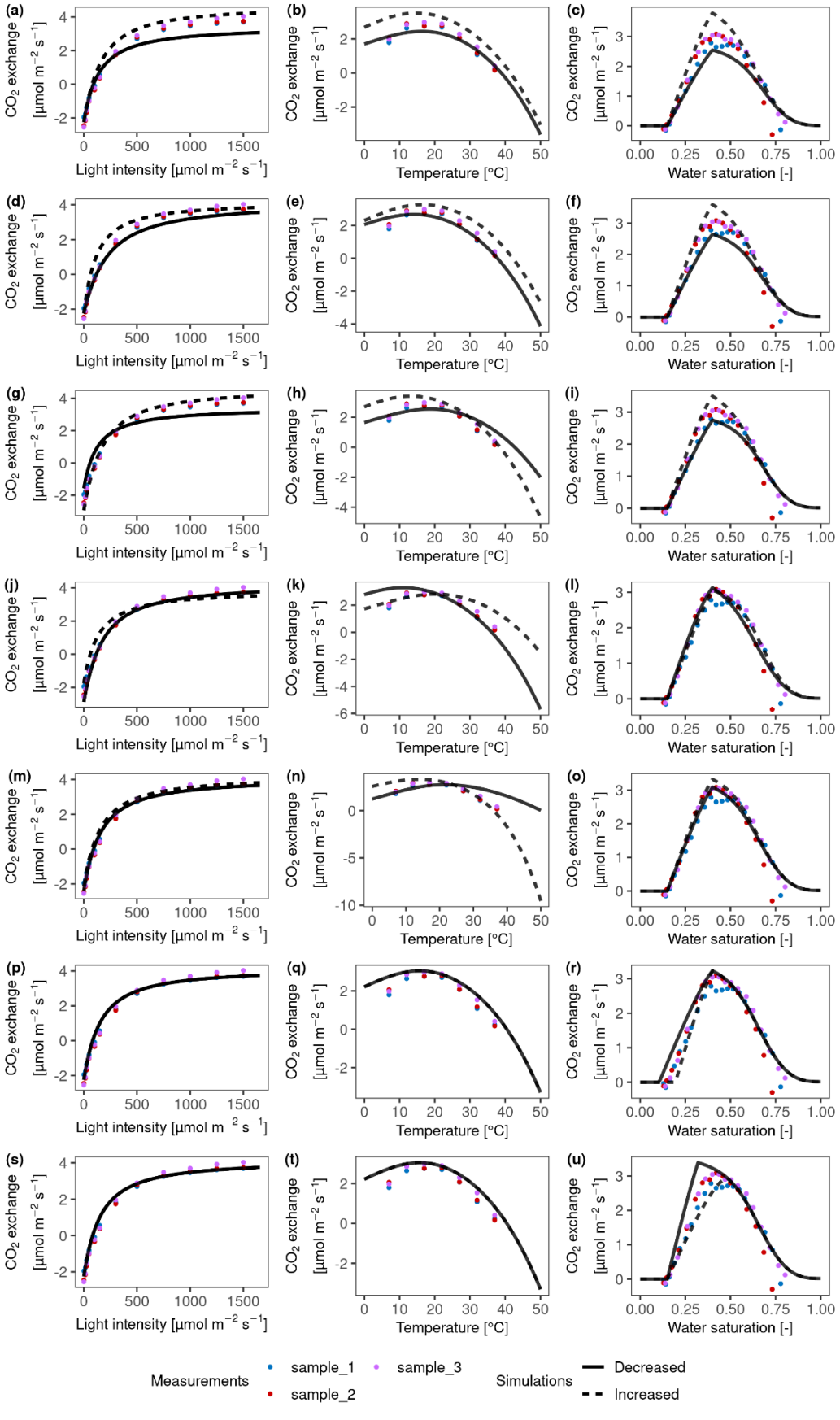

Figure S6: Simulated net photosynthesis rate in response to light (a, d, g, j, m, p, s), temperature (b, e, h, k, n, q, t) and water (c, f, i, l, o, r, u) at site D2 by the data-driven model with decreased or increased physiological parameters. These varying physiological parameters are respiration cost of RuBisCO enzyme (Rub_ratio) (a-c), light absorption fraction in cells (ExtL) (d-f), metabolic respiration cost per surface area (Resp_main) (g-i), the optimum temperature for gross photosynthesis (Topt) (j-l), Q10 value of respiration (q10) (m-o), minimum saturation for activation (Sat_act0) (p-r) and minimum saturation for full activation (Sat_act1) (s-u). Resp_main, ExtL, q10, Sat_act0 increased or decreased by 30%, Rub_ratio and Sat_act1 by 20%, and Topt by 5 K. The colored points represent the measured CO_2 exchange rates of different replicates of lichen-dominated biocrusts.

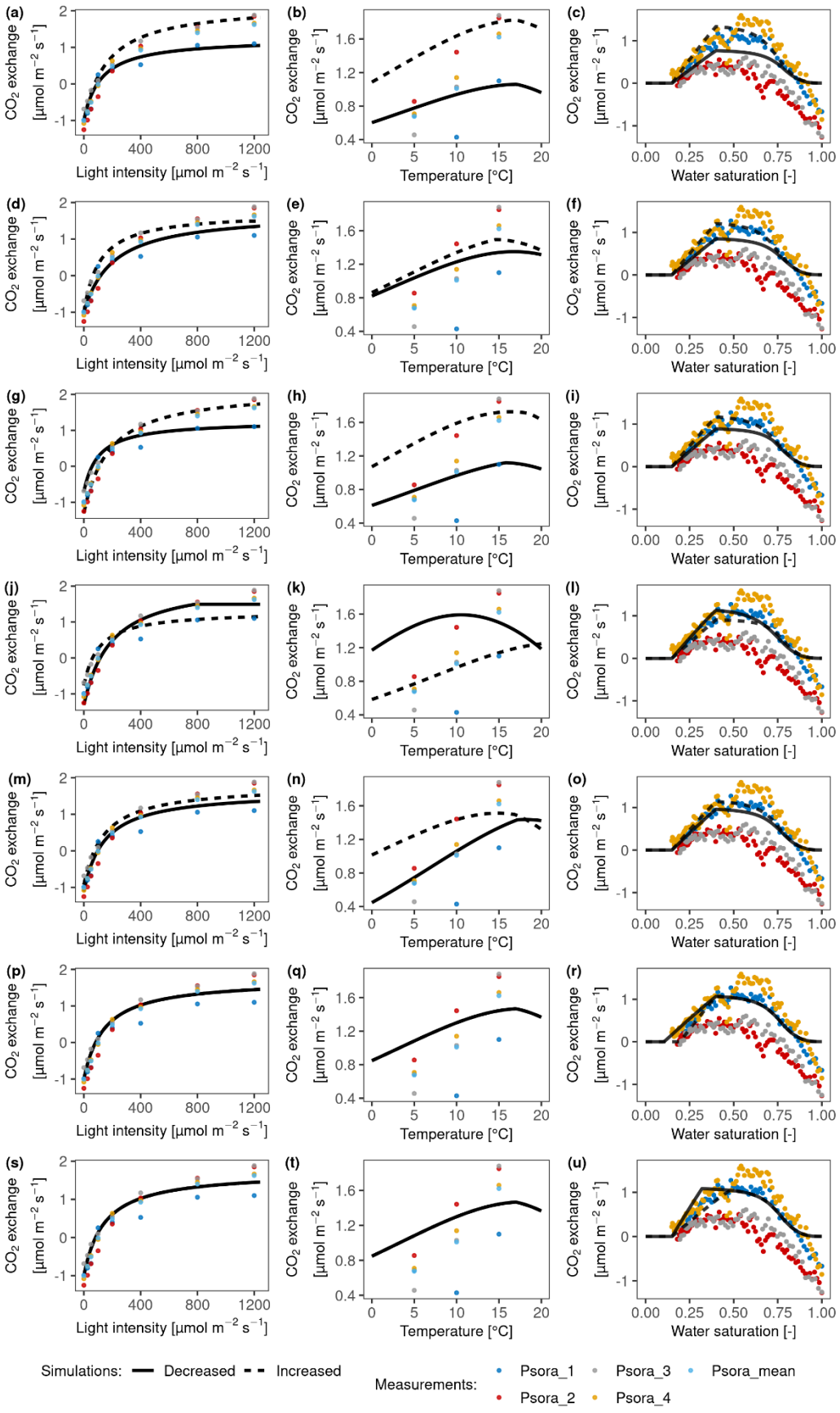

Figure S7: Simulated net photosynthesis rate in response to light (a, d, g, j, m, p, s), temperature (b, e, h, k, n, q, t) and water (c, f, i, l, o, r, u) at site T1 by the data-driven model with decreased or increased physiological parameters. These varying physiological parameters are respiration cost of RuBisCO enzyme (Rub_ratio) (a-c), light absorption fraction in cells (ExtL) (d-f), metabolic respiration cost per surface area (Resp_main) (g-i), the optimum temperature for gross photosynthesis (Topt)

(j-l), Q10 value of respiration (q10) (m-o), minimum saturation for activation (Sat_act0) (p-r) and minimum saturation for full activation (Sat_act1) (s-u). Resp_main, ExtL, q10, Sat_act0 increased or decreased by 30%, Rub_ratio and Sat_act1 by 20%, and Topt by 5 K. The colored points represent the measured CO_2 exchange rates of different replicates of lichen-dominated biocrusts.

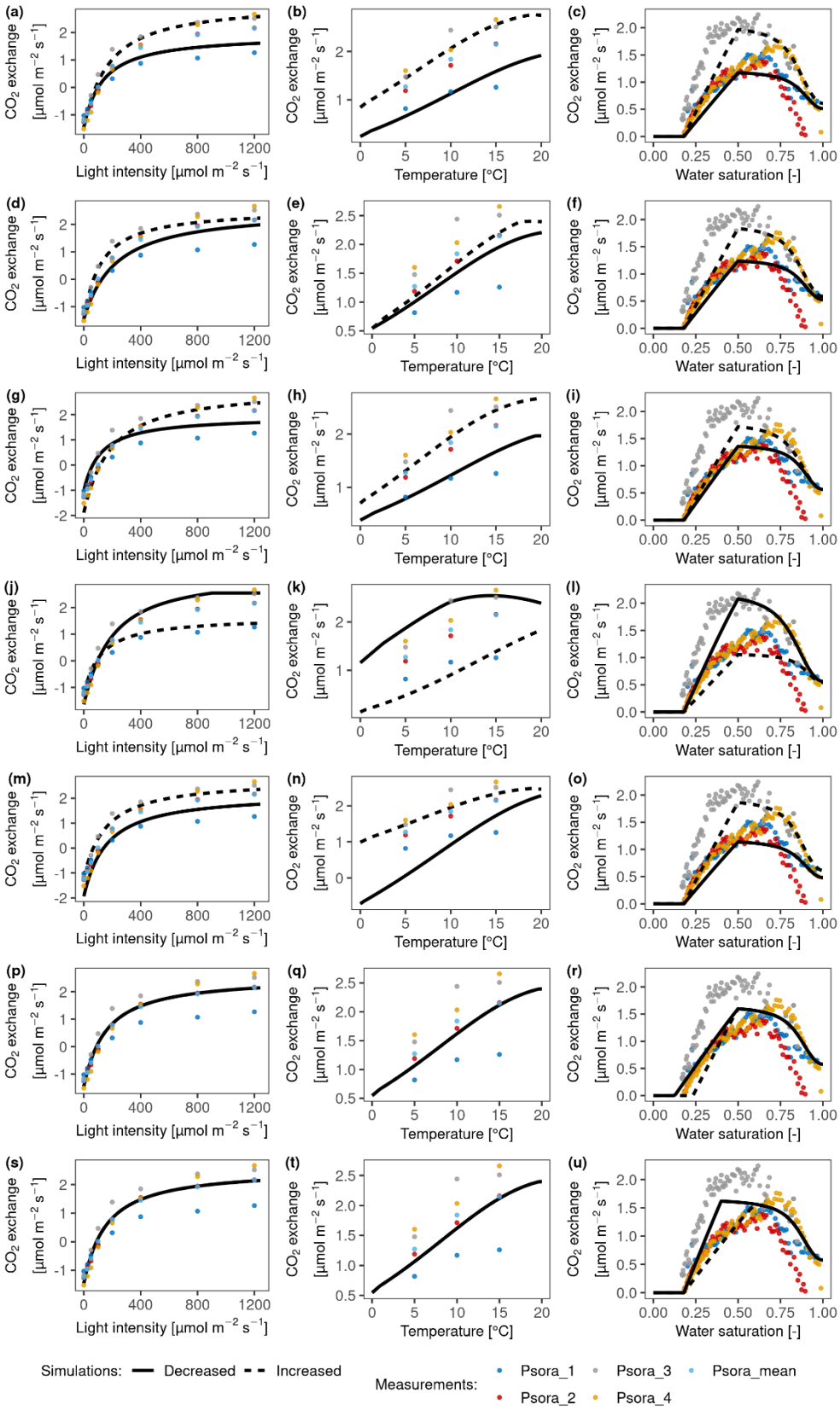

Figure S8: Simulated net photosynthesis rate in response to light (a, d, g, j, m, p, s), temperature (b, e, h, k, n, q, t) and water (c, f, i, l, o, r, u) at site T2 by the data-driven model with decreased or increased physiological parameters. These varying physiological parameters are respiration cost of RuBisCO enzyme (Rub_ratio) (a-c), light absorption fraction in cells (ExtL) (d-f), metabolic respiration cost per surface area (Resp_main) (g-i), the optimum temperature for gross photosynthesis (Topt) (j-l), Q10 value of respiration (q10) (m-o), minimum saturation for activation (Sat_act0) (p-r) and minimum saturation for full activation (Sat_act1) (s-u). Resp_main, ExtL, q10, Sat_act0 increased or decreased by 30%, Rub_ratio and Sat_act1 by 20%, and Topt by 5 K. The colored points represent the measured CO_2 exchange rates of different replicates of lichen-dominated biocrusts.

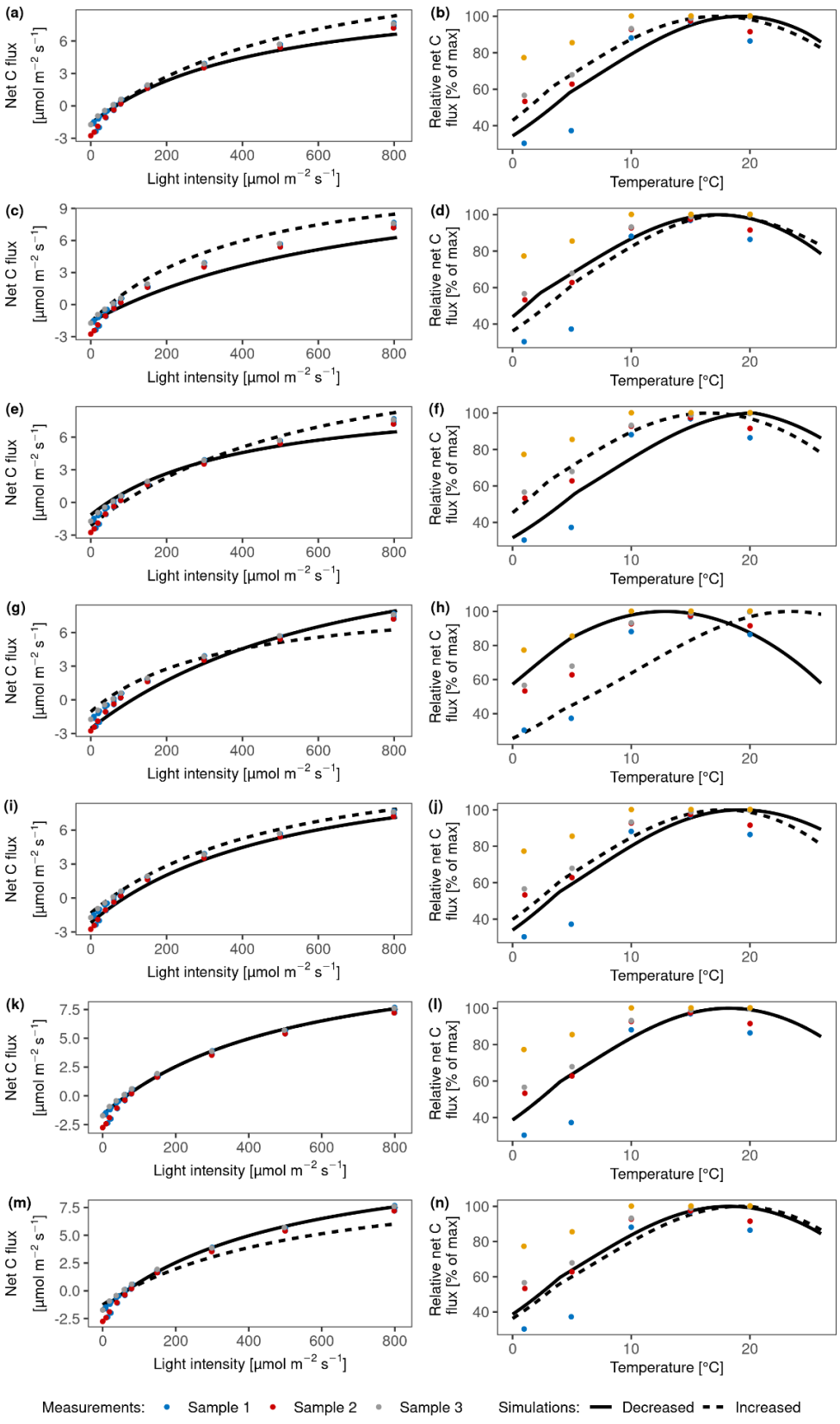

Figure S9: Simulated net photosynthesis rate in response to light (a, c, e, g, i, k, m) and temperature (b, d, f, h, j, l, n) at site T3 by the data-driven model with decreased or increased physiological parameters. These varying physiological parameters are respiration cost of RuBisCO enzyme (Rub_ratio) (a-b), light absorption fraction in cells (ExtL) (c-d), metabolic respiration cost per surface area (Resp_main) (e-f), the optimum temperature for gross photosynthesis (Topt) (g-h), Q10 value of respiration (q10) (i-j), minimum saturation for activation (Sat_act0) (k-l) and minimum saturation for full activation (Sat_act1) (m-n).

Resp_main, ExtL, q10, Sat_act0 increased or decreased by 30%, Rub_ratio and Sat_act1 by 20%, and Topt by 5 K. The colored points represent the measured CO_2 exchange rates of different replicates of lichen-dominated biocrusts.

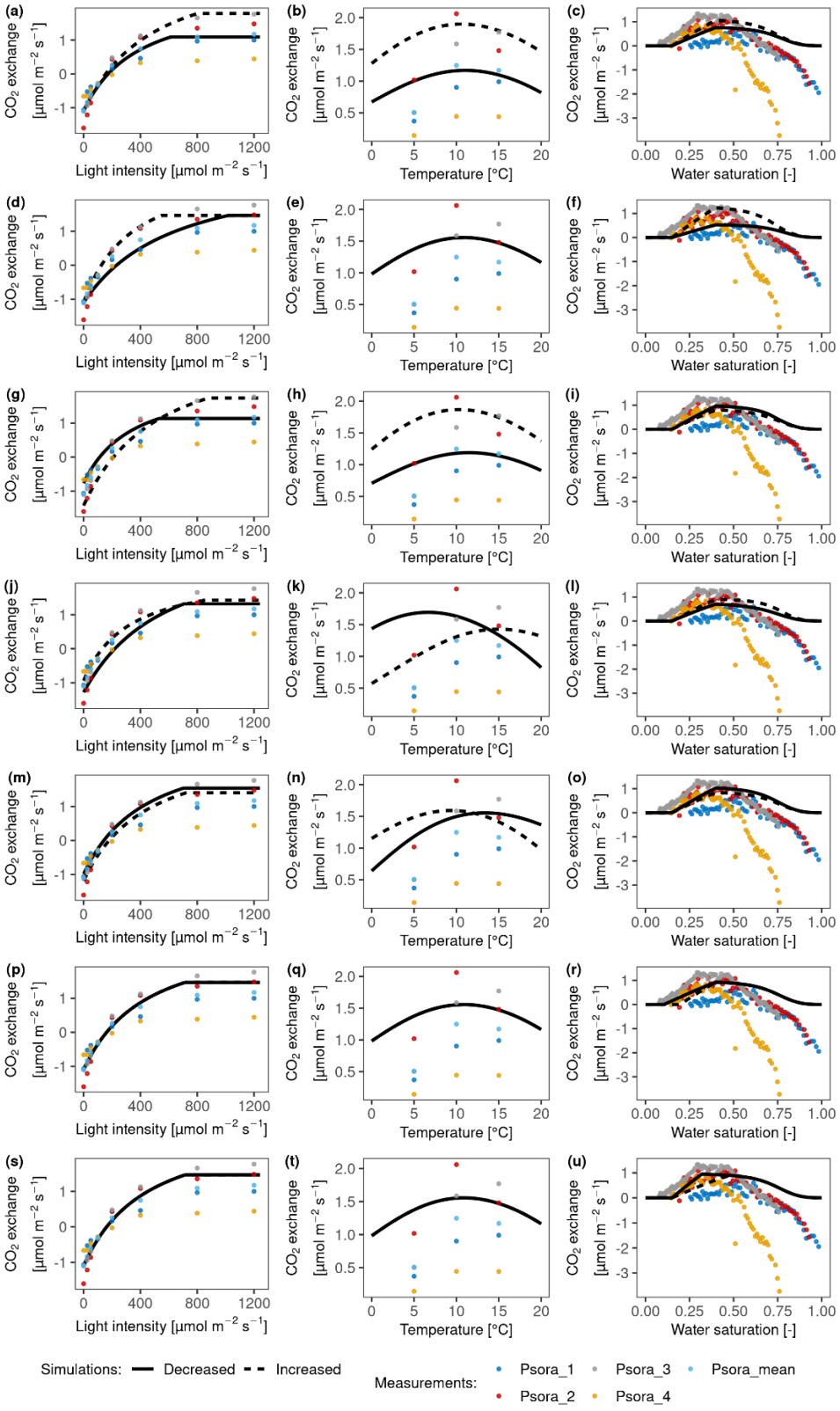

Figure S10: Simulated net photosynthesis rate in response to light (a, c, e, g, i, k, m) and temperature (b, d, f, h, j, l, n) at site A1 by the data-driven model with decreased or increased physiological parameters. These varying physiological parameters are respiration cost of RuBisCO enzyme (Rub_ratio) (a-c), light absorption fraction in cells (ExtL) (d-f), metabolic respiration cost per surface area (Resp_main) (g-i), the optimum temperature for gross photosynthesis (Topt) (j-l), Q10 value of respiration

(q10) (m-o), minimum saturation for activation (Sat_act0) (p-r) and minimum saturation for full activation (Sat_act1) (s-u). Resp_main, ExtL, q10, Sat_act0 increased or decreased by 30%, Rub_ratio and Sat_act1 by 20%, and Topt by 5 K. The colored points represent the measured CO_2 exchange rates of different replicates of lichen-dominated biocrusts.

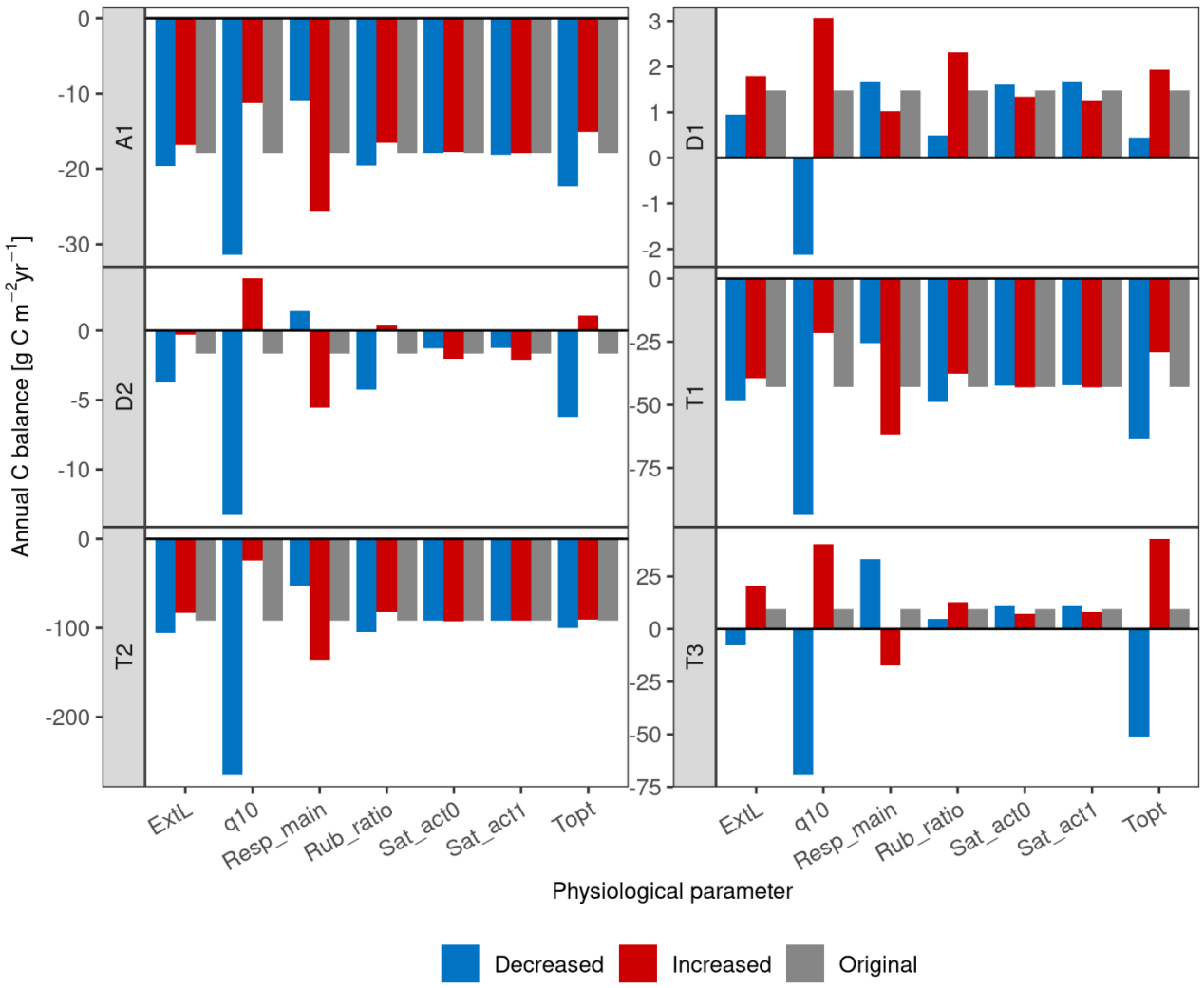

Figure S11: The C balance number estimated by the data-driven model without changing the parameters (Original), and with increasing and decreasing physiological parameters at all sites (Increased and Decreased, respectively). The changed parameters are respiration cost of RuBisCO enzyme (Rub_ratio), light absorption fraction in cells (ExtL), metabolic respiration cost per surface area (Resp_main), the optimum temperature for gross photosynthesis (Topt), Q10 value of respiration (q10), minimum saturation for activation (Sat_act0) and minimum saturation for full activation (Sat_act1). Resp_main, ExtL, q10, Sat_act0 increased or decreased by 30%, Rub_ratio and Sat_act1 by 20%, and Topt by 5 K.

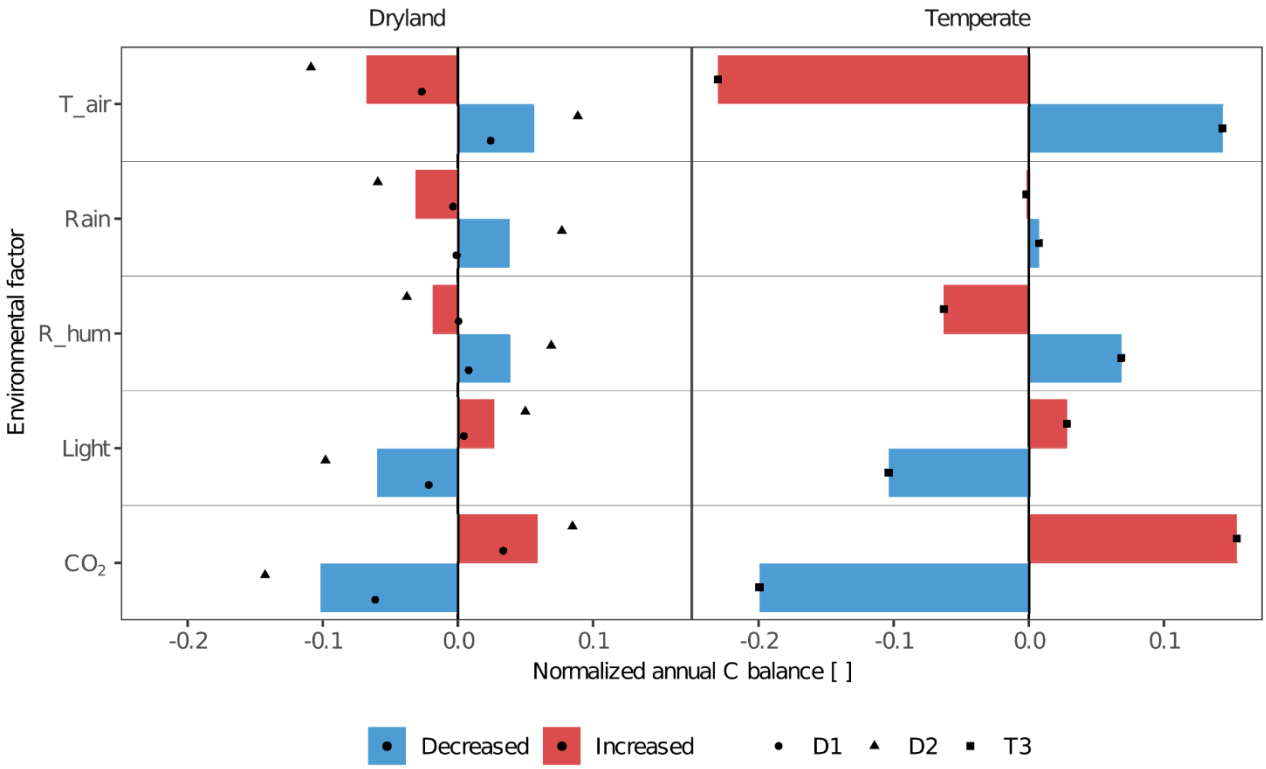

Figure S12: The effects of environmental factors - CO_2 concentration (CO_2), relative air humidity (R_hum), rainfall amount (Rain), air temperature (T_air) and light intensity (Light) on the annual C balance of lichen-dominated biocrusts at different sites with reasonable C balance estimates (excluding site T1, T2 and A1 with strongly negative C balance). The altered annual C balance resulting from increasing or decreasing environmental factors is normalized by the C balance under original environmental conditions. The colored columns indicate the average value of the normalized C balance at sites with similar climate conditions. Various styles of black points indicate different sites.

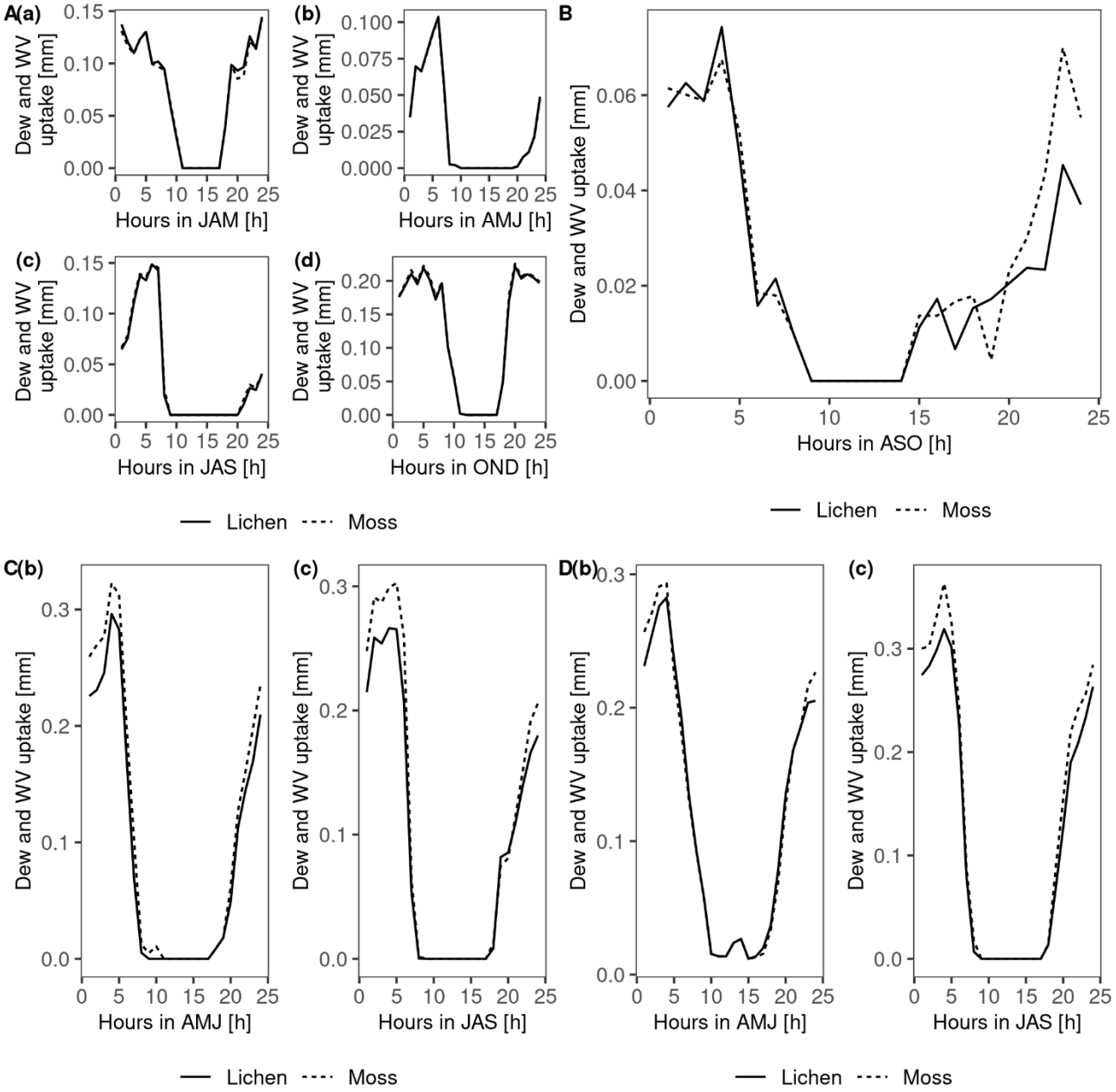

Figure S13: Modeled hourly sum of dew and water vapor uptake of lichen- and moss-dominated biocrusts at site D1 (A), T1 (B), T2 (C) and A1 (D) during seasons when an obvious underestimation of activity at night and morning can be observed. (a): diurnal pattern during the period January, February and March (JFM); (b): diurnal pattern during the period April, May and June (AMJ); (c): diurnal pattern during the period July, August and September (JAS); (d): diurnal pattern during the period October, November and December (OND); ASO represents August, September and October.

2 Details about the LiBry model

LiBry model was used to simulate the dynamics of non-vascular vegetation (including lichens, bryophytes, and cyanobacteria) at various research sites (Porada et al., 2013, 2014, 2017, 2018; Porada and Giordani, 2021). The LiBry model simulates the responses of a large number of physiologically and morphologically different strategies to environmental conditions and select strategies with optimal values for functional traits, adapting to the predefined climatic conditions. Each strategy is defined by a unique combination of parameter values and thus represents a group of functionally identical individuals. The physiological and morphological parameters of each strategy are photosynthetic capacity, thallus specific area, etc. The value of each parameter is randomly generated from their respective possible

ranges, which are derived from the literature, with trait combinations subject to biophysical and physiological constraints/trade-offs (see Porada et al., 2013). At the level of functional properties (traits), several similar strategies together may represent a species, thereby accounting for intra-specific trait variation.

The model is driven by a time series of climatic forcing data and other abiotic parameters describing the habitat, such as disturbance interval, the surface roughness length, etc. Some of the abiotic parameters can be derived more easily by calibration. Parameters like roughness length, soil thermal conductivity, or soil heat capacity, for instance, are calibrated through the fitting of model equations concerning water and energy fluxes to daily and diurnal patterns of measured surface temperature and moisture. A large number of strategies with combinations of the different parameter values are generated by the model before the start of the simulation. Then the carbon dynamics of each strategy is calculated based on physiological and biochemical mechanisms during simulations. For example, an organism gains carbon through photosynthesis and releases it by respiration. The gross photosynthesis rate is calculated based on the Farquhar photosynthesis scheme (Farquhar and von Caemmerer, 1982); respiration is temperature-dependent (Q10 relationship). Both photosynthesis and respiration depend on the water saturation of the strategy, which is regulated through the input rainfall, snowmelt, dewfall, and evaporation. The evaporation and dew are calculated via the energy balance approach, the negative energy balance leads to condensation at the surface and thus the dewfall. Unlike vascular plants that have stomata, biocrusts are poikilohydric, and cannot actively control water exchange. Uptake (or loss) of water from (or to) the air in the model depends on the net radiation and vapor pressure deficit. The vapor pressure deficit is the difference between saturation water vapor pressure at the surface corrected by water potential inside the biocrust thallus and the atmospheric water vapor pressure which is related to relative humidity.

The C balance then translates into biomass, resulting in growth in cover if this translated biomass is larger than the biomass lost due to tissue turnover, whereas a negative C balance, as well as disturbance, leads to mortality, and thus a shrinkage of the cover. In the end, the strategies that have a positive cover area in the long term survive in the model. In other words, the survival of strategies is determined by their C balance.

The LiBry model ran for 300 years to simulate the dynamics of generated 1000 strategies. The input of such a large number of strategies is to ensure that the combinations of all possible values of all functional traits in research sites are considered for selection by the LiBry model.

3 Supplementary analyses

3.1 Calibration

3.1.1 Fitting of surface temperature

The abiotic surface properties required by the data-driven model are obtained by fitting the daily and diurnal surface temperature to measurements. The results showed early peaks at site T1, T2, D1 and A1 and underestimation in several seasons. For instance, from January to March at site T2 (Fig. 1 (b)). This may result from the measured diurnal patterns of PAR or air temperature at 2 m being inconsistent with the measured surface temperature. We compared the diurnal patterns of the measured PAR, surface temperature (Measured_Ts) and air temperature at 2 m (Tair), and simulated surface temperature (Simulated_Ts) from January to March and found the different measured climate variables might have uncertainties against each other. For instance, Tair has an earlier increase than Measured_Ts, which is unusual, and also is always lower than Measured_Ts, even at night, which could partly explain the underestimated surface temperature there (Fig. S14 (a)). When we shifted the PAR data to 1 hour later, we found that the early peak of simulated surface temperature is corrected (Fig. S14 (b)).

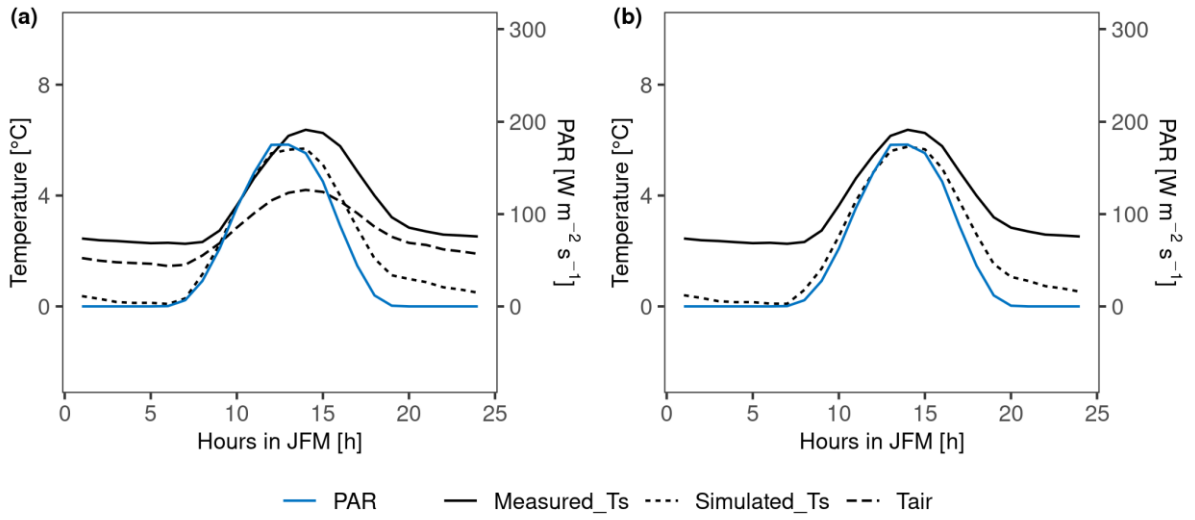

Figure S14: The diurnal patterns of PAR, measured surface temperature (Measured_Ts), measured air temperature at 2m (Tair), and simulated surface temperature (Simulated_Ts) from January to March at site T2. (a): The patterns of original measurements and simulation. (b): the patterns of measured variables and simulated surface temperature when PAR was shifted to 1 hour later.

Furthermore, the calibrated boundary parameters such as soil thermal conductivity in the model could affect the diurnal temperature difference, and thus partly lead to the mismatches in diurnal surface temperature patterns, although do not have a strong influence on the timing of the peak in surface temperature. A sensitivity analysis of soil thermal conductivity was conducted at T1 to check whether the bias in calibrated boundary parameters can have a large impact on the carbon balance of biocrusts. The results showed that changing soil thermal conductivity does not prevent a negative carbon balance value in the model (change from -42.8 to -37.1 and to -50.9 g C m^{-2} yr^{-1}, respectively, for lichen-dominated biocrust when soil thermal conductivity increased or decreased 5 times).

3.1.2 Fitting of photosynthesis response curves

In the calibration of physiological properties, we can, however, only reduce the net photosynthetic rate close to 0 at high water saturation, but it is impossible to fit the strongly negative net C flux there.

The reason are the CO_2 diffusion pathways implemented in our data-driven model. We assume that CO_2 only leaves the thallus through the same route as it enters. Furthermore, we assume that the net flux between the interior of a lichen/bryophyte and the atmosphere has the same magnitude as the flux (respiration minus photosynthesis; see Fig. S15). This "steady-state" assumption is similar to vascular vegetation models and is justified by the comparably small internal space for CO_2 storage which prevents long-term (meaning minutes) maintenance of photosynthesis under insufficient influx of CO_2. These assumptions do not allow the simulation of a negative net C flux under the relatively high light of the response curve setup (see also Fig. S15 (a)). As the measured response curves show, the net C flux of one sample of lichen-dominated biocrust at high water saturation (Fig. 2 (c)) is similar to the dark respiration rate obtained from the light-response curve (Fig. 2 (a)), meaning that, for this sample, the flux of CO_2 out of the thallus to the atmosphere at high water saturation is likely similar in magnitude to respiration rate. In this case, the gross photosynthesis rate of the sample is likely approximately zero. But, in the model, the CO_2 concentration inside the thallus needs to be larger than the atmospheric CO_2 (400 ppm) in order to achieve a negative net flux. The relatively high CO_2 concentration together with the ambient light level of 400 µmol m^{-2} s^{-1} in the experimental setup of the water response curve, force the modelled gross photosynthesis rate to markedly exceed zero, and therefore it is impossible to achieve a large negative net C flux with the model.

The only way to simulate a negative net C flux under light is to assume that the largest part of CO_2 leaves the thallus via a different route (Fig. S15 (b)). In this case, the small flux of CO_2 from the atmosphere into the thallus at high water saturation and further into the chloroplasts, which leads to little gross photosynthesis, is overcompensated by a much larger respiration flux that directly enters the atmosphere through a different route. However, this is highly uncertain and also a bit questionable for most lichens and bryophytes. It may be possible in a lichen if the organism has a high amount of fungal biomass located above the photobionts that contain the chloroplasts, but without detailed information on the morphology, this would represent an arbitrary parametrization. Alternatively, we would have to assume that respiration of the sample in Fig. 2 (c) is substantially higher than in Fig. 2 (a), but this seems arbitrary, too.

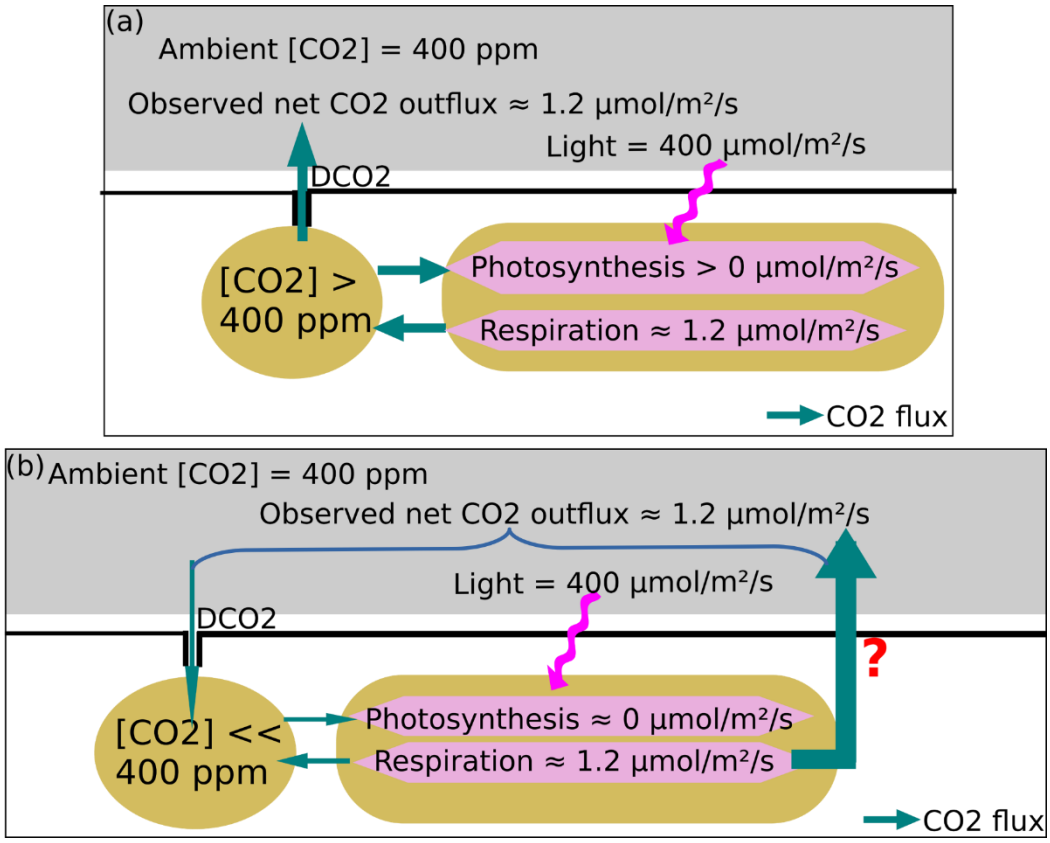

Figure S15: The schematic diagram of the CO_2 diffusion pathways. (a): the pathway in the data-driven model, which makes it impossible to fit a strongly negative net C flux. (b): The pathway that allows a simulation of strongly negative net C flux. Please note that the figure only shows CO_2 fluxes. Contrary to vascular plants, CO_2 and water exchange are not coupled in lichens and mosses, due to lack of stomata. The model thus calculates water fluxes independently based on the surface energy balance.

3.2 Effect of MWC on C balance

The estimated C balance may be inaccurate due to potential bias in estimated relative water saturation, which partly depends on prescribed MWC, a morphological model parameter that is obtained by measurements. We varied the MWC of lichen-dominated biocrust from site T1 by half (+/- 50%) to examine how important uncertainty in this parameter is for the estimation of the C balance. The outcome revealed that MWC has little effect on C balance (-40.0, -42.8, -44.5 g C m-2 yr-1 for reduced, original and increased MWC). Therefore, the annual carbon estimation is robust to the uncertainties with regard to the prescribed MWC.

4 References

Farquhar, G. D. and von Caemmerer, S.: Modelling of Photosynthetic Response to Environmental Conditions, in Physiological Plant Ecology II, edited by O. L. Lange, pp. 549–587, Springer, Berlin, Heidelberg., 1982.

Porada, P. and Paolo, G.: Bark Water Storage Plays Key Role for Growth of Mediterranean Epiphytic Bark Water Storage Plays Key Role for Growth of Mediterranean Epiphytic Lichens, Front. For. Glob. Chang., 4, 30, doi:10.3389/ffgc.2021.668682, 2021.

Porada, P., Weber, B., Elbert, W., Pöschl, U. and Kleidon, A.: Estimating global carbon uptake by lichens and bryophytes with a process-based model, Biogeosciences, 10, 6989–7033, doi:10.5194/bg-10-6989-2013, 2013.

Porada, P., Weber, B., Elbert, W., Pöschl, U. and Kleidon, A.: Estimating impacts of lichens and bryophytes on global biogeochemical cycles, Global Biogeochem. Cycles, 28(2), 71–85, doi:10.1002/2013GB004705.Received, 2014.

Porada, P., Pöschl, U., Kleidon, A., Beer, C. and Weber, B.: Estimating global nitrous oxide emissions by lichens and bryophytes with a process-based productivity model, Biogeosciences, 14, 1593–1602, doi:10.5194/bg-14-1593-2017, 2017.

Porada, P., Van Stan II, J. T. and Kleidon, A.: vegetation to global rainfall interception, Nat. Geosci., 11, 563–567, doi:10.1038/s41561-018-0176-7, 2018.